Behavior of earthquake-resistant structure elements using polypropylene fiber and high strength reinforcing bars

Maulana Derry Imansyah[1,*], *Iswandi* Imran[2], *Kurniawan S.* Kamaruddin[1], *Aris* Aryanto[2], and *Muhammad* Riyansyah[2]

[1]Post Graduate Program of Faculty of Civil Engineering, Bandung Institute of Technology, 40132 Bandung, Indonesia
[2]Structural Engineering Department, Faculty of Civil Engineering, Bandung Institute of Technology, 40132 Bandung, Indonesia

Abstract. The use of high strength reinforcing bars has becoming an interesting and cost-efficient option in construction industry recently. However, their use is limited due to their low deformability which might induce a brittle collapse in the structures. Also, longer development length is needed to transfer stress from reinforcing bars to the surrounding concrete. This paper focuses on investigating the influence of fibrous concrete and high-strength reinforcing bars on the behavior of structural elements. Five half-scaled specimens of interior joints using plain or fibrous concrete, reinforced with conventional 420 MPa or high strength reinforcing bar of 520 Mpa were experimentally tested. The two specimens of plain concrete, reinforced longitudinally with 16 mm and 19 mm reinforcing bars are defined as control specimens. The other test specimens were casted with Polypropylene fiber reinforced concrete (PFRC) with 16 mm and 19 mm longitudinal reinforcing bar. Loading protocol of all test specimens is defined according to ACI 374.2. The structure behavior, such as dissipated energy, bond between reinforcing bars and surrounding concrete, and stiffness degradation of the four specimens were evaluated and compared. The results obtained shows that the use of fiber increase the dissipated energy up to 27.5 % compared to specimens with plain concrete. Moreover, the peak strength of PFRC specimens was slightly increased (3% - 7%) compared to that of specimens with plain concrete. Moreover, there is an increase in peak-to-peak stiffness at elastic range loading with the addition of fiber, while no significant difference after the yields of longitudinal reinforcing bars.

1 INTRODUCTION

In Indonesia, reinforcing bars with the yield strength of 420 MPa is widely used in construction industry. Current provisions in Indonesia that regulating this industry only allow reinforcing bars up to 420 MPa in yield strength for longitudinal bars in structural elements. All of those provisions are intended to ensure the desired behavior of structure can be achieved. The behavior of structure under seismic loads must be taken as an important aspect in design phase, considering that Indonesia is located at seismically active region surrounded by 3 earth plates, i.e. Eurasian, Pacific, and Indo-Australian Plate.

In the other hand, demand for sustainable and cost-saving materials in this industry is increasing recently. One of the product that found to be interesting is high strength reinforcing bars. Utilization of this material in structural elements can greatly alleviate the rebar congestion, weight of material used, cost of material handling and storing, etc.

The problem of this concept is, high strength reinforcing bar is notoriously has some drawbacks as it dissipates less energy and lower ductility compared to conventional reinforcing bar with yield strength of 420 MPa. Increasing the yield strength of reinforcing bars embedded in concrete resulting in increased developing length, i.e. length needed to transfer yield tensile strain from rebar to surrounding concrete. It can negatively affect the bond behavior between concrete and reinforcing bars. Some researches need to be done in order to ensure that the seismic behavior of high strength reinforced concrete is still acceptable.

In the recent decades, material technology of concrete for construction has advancing rapidly. Researches for concrete material have been developing alternatives to improve the material's properties and behavior. Fiber-reinforced concrete was a product of those researches that could improve several behavior of concrete. Fiber used as reinforcement for concrete comes in many shapes and materials, whether straight or hooked, and natural or polymer. Most of the research conducted in recent decades was focused on the application of steel and polypropylene fiber. Studies conducted by many researchers (for example, Osorio et al. [1], Ramakrishnan et al. [2], Wafa et al. [3], Jie et al. [4]), found that the addition of fiber into concrete matrix can enhance the post-peak behavior and, thereof, the ductility and energy-dissipation capacity of structural elements. Huang et al. [5], reported that fiber RC specimens, with the addition of

* Corresponding author: maulanaderry@gmail.com

polypropylene and steel fiber at different percentage, have shown better bond performance. The use of fibrous concrete in beam column joint also conducted by several researcher [6] [7] [8]. Yet, the structural application of fiber-reinforced concrete is currently limited as it still needs any further research.

The objective of this research is to study the effect of the addition of polypropylene fiber in an interior beam-column joint reinforced by high strength reinforcing bar. The addition of polypropylene into structural elements reinforced with high strength bars is supposed to compensate the negative effect of the application of the bars mentioned above. Change of stiffness, energy dissipation, and ductility of this structural element is sought.

2 EXPERIMENTAL PROGRAM

2.1 Test Specimens

In this study, five interior beam column joints scaled in half were tested under reversed lateral cyclic loads. Each specimen was 1.6 m in height and a total of 3 m in width, with 1.325 m clear span of both beams. The specimens divided into 3 groups based on the yield strength and diameter of longitudinal rebar, and the addition of fiber into concrete mix. The first group consisted of a specimen reinforced longitudinally with D16, yield strength of 420 MPa rebar and casted with plain concrete. This specimen is defined as control specimen, representing the current materials used in construction. The second group has rebar yield strength of 520 MPa, consisted of two different rebar diameter, i.e. D16 and D19, casted with plain concrete. The last group was similar to the second group, with the addition of fiber in the concrete matrix. Polypropylene fiber added into concrete mixture at 0.5% volume fraction per m^3. Materials used for each test specimen is given in Table 1.

Table 1. Material properties of beam-column joint specimens

Group	Specimen	Longitudinal Reinf.		PP Fiber
		Yield Str. (MPa)	Diameter (mm)	
1	D16-400N	420	16	0%
2	D16-500N	520	16	0%
	D19-500N		19	0%
3	D16-500F	520	16	0.50 %
	D19-500F		19	0.50 %

2.2 Material Properties

Two different strengths conforming ASTM A615M [9] [10] of reinforcing bars were used in this study. For control specimen, conventional 400 MPa with diameter of D16 was used as reinforcing bars. Four other specimens were reinforced by 520 MPa bars with diameter of D16 and D19. Concrete with compressive strength of 30 MPa was used for all specimens, with the addition of fiber in third specimen group as shown in table 1. Mechanical properties of each material are shown in table 2 and 3. The mechanical properties of reinforcing bars were obtained from tensile strength test of 2 sets of specimens by yield strength (i.e. 420 MPa and 520 MPa), consisted by 4 specimens each. The test was conducted according to ASTM A370.

Table 2. Mechanical properties of reinforcing bars

Material	Sectional Area (mm^2)	Yield Str. (MPa)	Tensile Str. (MPa)	Young Modulus (Gpa)
D16	201.06	434.1	577.4	198.1
	201.06	485.2	630.9	207.9
D19	283.53	503.9	674.9	195.7

Compressive strength test of concrete material was conducted on 3 plain concrete and 2 fibrous concrete specimens. The compressive test was carried at 28 days after casting. Note that a slight reduction of 6.8% in compressive strength was measured with the addition of polypropylene fiber.

Table 3. Mechanical properties of plain and fibrous concrete

Material	Compressive Str. (MPa)
fc' 30 MPa	31.78
fc' 30 MPa PPF	29.61

2.3 Design of Specimens

All specimens are designed as an element of Special Moment Resisting Frame, according to SNI 2847-2013 clause 21.5. Each specimen is consisted of a 350x350mm column and 150x250mm beam. The column was reinforced by 8 longitudinal bars, with different diameter as stated in table 1. Reinforcement ratio of column was 1.31% for specimens with D16 bars, and 1.85% for specimens with D19 bars. For confinement and shear reinforcement, all of the specimens used D10 bars with 80mm spacing.

For specimens with D16 reinforcing bars, different amount of reinforcing bars was used as top and bottom longitudinal reinforcement of the beams. Top layer of the section was reinforced by 3-D16 bars, while bottom layer was reinforced by 2-D16 bars. While for D19 specimens, longitudinal reinforcing bars were symmetrical between top and bottom layer with 2-D19 bars. High overstrength ratio of specimen's column and beam component, with magnitude ranging from 2-3 was used in order to ensure that all specimens end up with failure of both beams rather than the column failure. All of the specimens used D10 bars with 55mm spacing as confinement or shear reinforcement. High degree of shear reinforcement was used to prevent

* Corresponding author: maulanaderry@gmail.com

shear failure of the beam. Reinforcement cages of all specimens are illustrated in Figure 1.

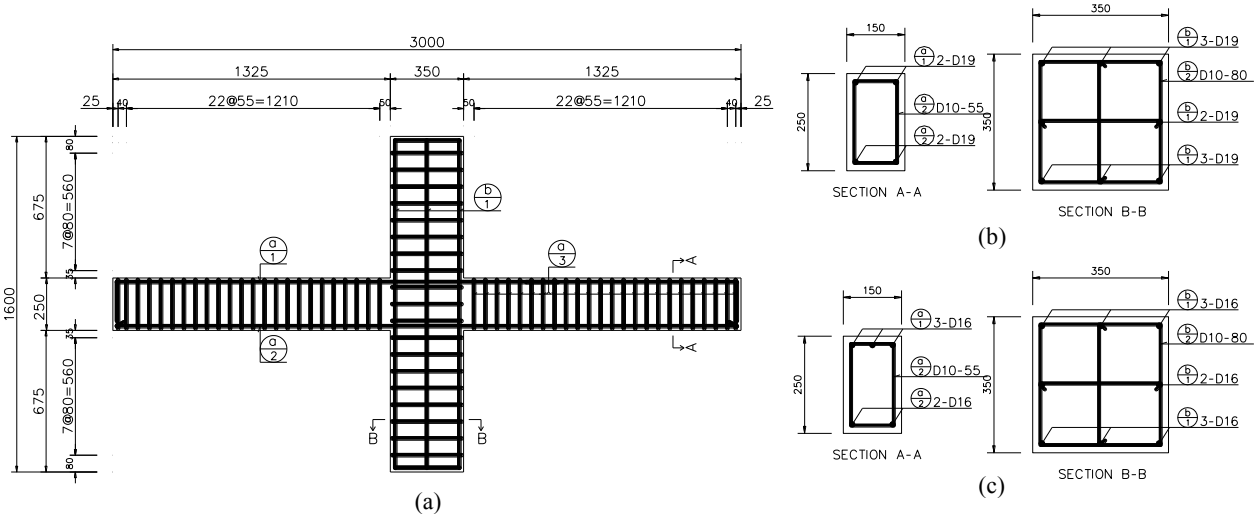

Figure 1. Reinforcement detail of all specimens, (a) elevation view of specimen's reinforcing bars, (b) beam and column section for D19-500N and D19-500F specimens, (c) beam and column section for D16-400N, D16-500N, and D16-500F specimens

2.4 Test Instrumentation

A total of 26 channels were used for measuring the behavior of specimens under reversed cyclic loads. Instrumentation of the specimens focused mainly on the joint region and along plastic hinge of beams. Drift of the column was measured by four Linear Variable Displacement Transformer (LVDT) along the height of specimen. Rotation and shear deformation of plastic hinge region was measured by a total of 8 LVDT, as illustrated in Figure 2.

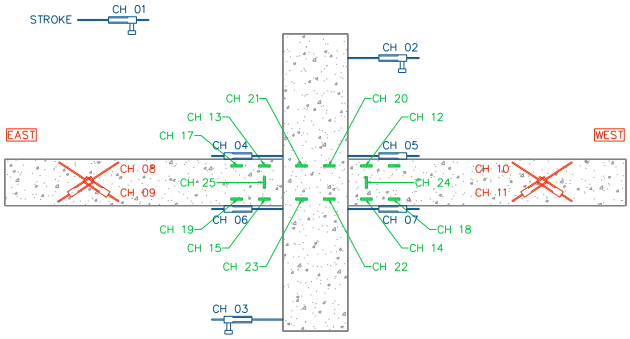

Figure 2. Instrumentation of the specimen tested

In the joint region, 14 strain gauges were used for measuring longitudinal and transversal reinforcement. Four strain gauges were placed inside the joint to obtain the bond behavior in this region, and the rest were placed in plastic hinge region of the beam. A total of 8 strain gauges attached to longitudinal reinforcement, and 2 strain gauges measuring the transverse reinforcement strain. Measurement of force applied was taken by the internal load cell of the actuator. Measurement taken by LVDT, strain gauges, and load cell were sent to data logger to be stored at computer. Reading of all channels was taken every 4 seconds approximately.

In addition to the utilization of LVDTs and strain gauges, several observation of the specimen's behavior were done manually. Crack propagation of the specimens were plotted and documented at every peak, followed by measurement of crack width using feeler gauge. Important events, such as first crack and spalling of concrete cover were recorded through the test.

2.5 Test Setup and Loading Protocol

Column of the specimens was restrained as pin at its both end, while both of the beams end were restrained to vertical movement, and released to lateral and rotational movement. This test setup was designed to reproduce the lateral behavior of beam column joint in real moment frames structure. Lateral load then applied to the top pin of column, displacement-controlled, using 100 kN DARTEC Loading Frame. The test setup and loading history of the specimens are shown in figure 3 and 4, respectively.

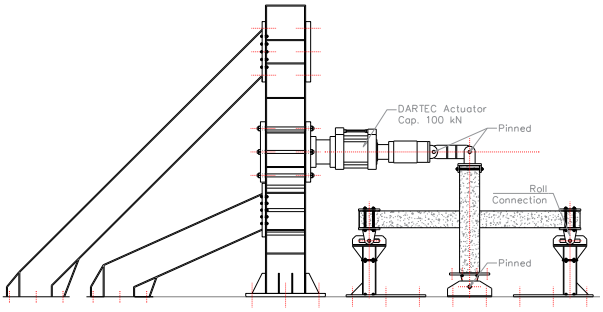

Figure 3. Test setup for beam column joint specimens

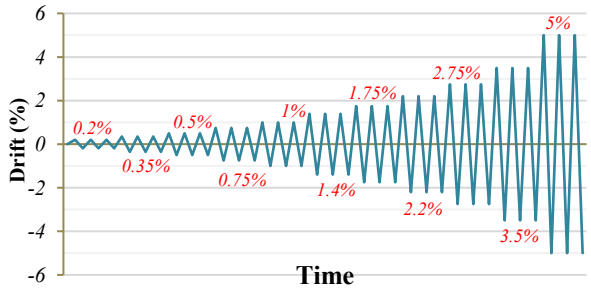

* Corresponding author: maulanaderry@gmail.com

Figure 4. Loading history of specimens

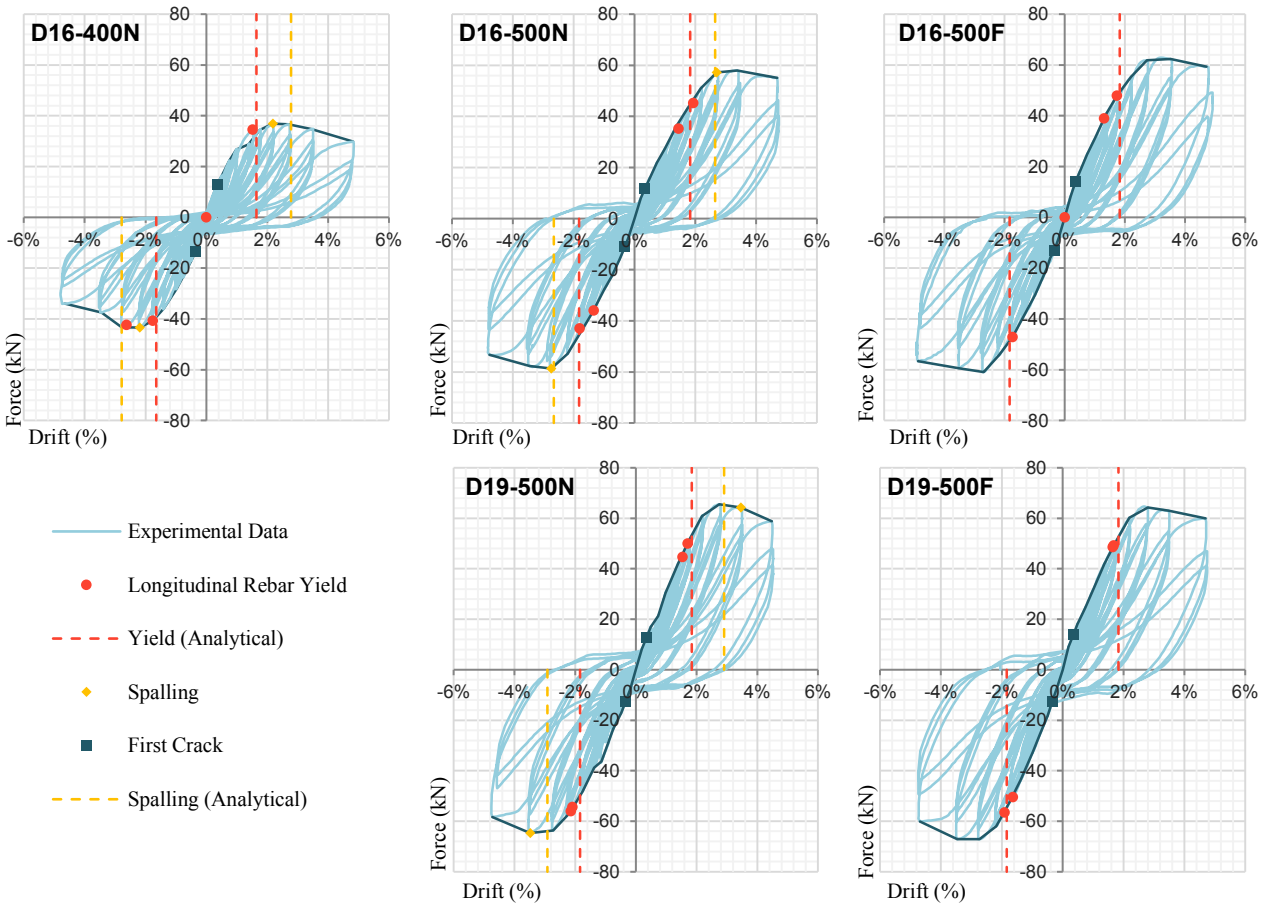

Figure 5. Comparison of experimental hysteretic curves for all specimens

All specimens subjected to displacement controlled, reversed cyclical load according to ACI 374.2. The tests were conducted in absence of axial load on column in order to obtain conservative result. Lateral loading of the specimens consisted of 11 increasing drift level ranging from 0.2% to 5%. Rate of loading was increased every 2 drift levels, ranging from 0.025 at the beginning of the test, to 0.25 mm/s at the 11th drift level. Each of those cycles was repeated 3 times before advancing to the next drift level. Each drift level was increasing in the magnitude of 1.25 to 1.5.

3 TEST RESULT AND DISCUSSION

All specimens were subjected to 66 cycles with increasing drift up to 5%. Despite all specimens were heavily damaged at the end of cyclical loading at drift ratio 5%, no failure has observed to occur. Hysteretic curve of load versus drift for all specimens are shown in Figure 5. Important events recorded such as first crack, significant yield, and spalling of the specimens are compared in Table 4.

Yield point in the positive direction of D16-400N specimen is left blank, as the strain gauge measuring strain of the beam's top west rebar was malfunctioned since the beginning of the test. No cover spalling was observed to happen in the specimens with fibrous concrete. It should also be noted, although the first crack of all specimens occurred at the same drift level, crack formed in the two fibrous concrete specimens were much less in length compared to specimens with plain concrete, suggested that fibrous concrete has higher tensile strength over plain concrete.

3.1 Backbone Curve

Comparisons of backbone curve for all specimens are shown in Figure 6 and Figure 7. From the backbone comparison graph, substitution of conventional 400 MPa to 500 MPa rebar gives a significant improvement in lateral load capacity, measured 35.18% over control specimen. Increasing the yield strength of rebar was not compensated by the reduction of rebar area in both beam and column section.

The addition of polypropylene fiber into concrete matrix yields a slight improvement in peak lateral load capacity. Improvement in peak strength from D16-500N to D16-500F specimens measured was 8.2% and 4.5% for positive and negative loading direction respectively. Improvement can also be found on D19-500F specimens in negative loading direction measured 5.65%, while positive loading direction shows a slight reduction in the peak lateral load. This reduction could be due to an offset of force measured by the load cell,

* Corresponding author: maulanaderry@gmail.com

i.e. the load cell gives a shift in force reading initiated from the beginning of the test towards negative value.

The exact values of the peak lateral load can be found in Table 4 and Table 5.

Table 4. Summary of test events for all specimens

Specimens	First Crack		Significant Yield		Spalling	
	Drift (%)	Force (kN)	Drift (%)	Force (kN)	Drift (%)	Force (kN)
D16-400N	0.353%	12.996	-	-	2.182%	36.843
	-0.350%	-13.526	-1.762%	-40.779	-2.194%	-43.346
D16-500N	0.350%	11.808	1.934%	45.164	2.703%	57.222
	-0.313%	-11.038	-1.806%	-43.066	-2.733%	-58.621
D16-500F	0.360%	14.075	1.736%	47.796	-	-
	-0.351%	-13.306	-1.735%	-47.173	-	-
D19-500N	0.341%	12.506	1.535%	44.586	3.451%	64.286
	-0.340%	-12.645	-2.088%	-54.384	-3.485%	-64.704
D19-500F	0.346%	13.816	1.647%	48.568	-	-
	-0.340%	-12.547	-1.635%	-50.480	-	-

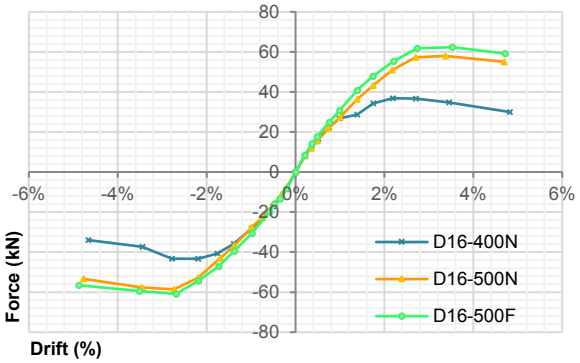

Figure 6. Force-drift backbone curve comparison for group 1 and 2 specimens

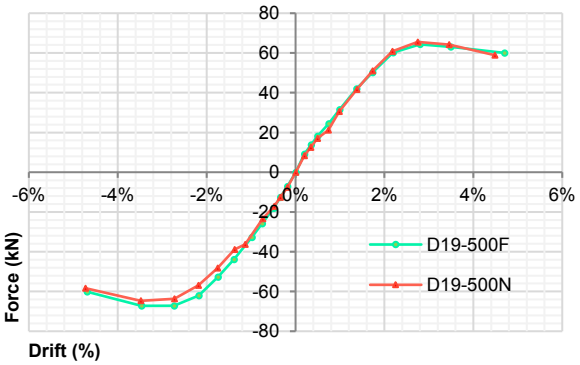

Figure 7. Force-drift backbone curve comparison for group 3 specimens

Table 5. Peak load comparison of backbone curves for all specimens

Specimens	Ultimate Force (kN)	
	(+) dir	(-) dir
D16-400N	43.346	36.843
D16-500N	58.621	57.991
D16-500F	60.856	62.355
D19-500N	64.704	65.555
D19-500F	67.172	64.325

* Corresponding author: maulanaderry@gmail.com

The improvement of peak lateral load could be related to the presence of concrete cover spalling in the specimens casted with plain concrete, considering that for both D16-400N and D16-500N the peak lateral load coincides with the spalling of the concrete cover, and initiating the reduction of the lateral load strength. The effect of concrete cover spalling was found to be lesser in the D19-500N specimen due to greater rebar area in compression part of the beam 2-D19 in comparison with 2-D16 rebar.

3.2 Dissipated Energy

Energy dissipated by the specimen was calculated by the area enclosed in hysteretic curves, which bigger area denotes the greater energy was dissipated. The hysteretic and backbone curves shown for each specimen in Figure 5 to Figure 7 are not comparable due to significant difference in yield force and displacement. Hence, to make the hysteretic and backbone curve comparable, scaling for force and displacement axis is needed. Adjustment for the difference between each specimen is represented with significant yield point.

The significant yield point, in which the normalization of the curve adjusted, is defined by ACI 374.2-13. Initial stiffness of the backbone curve is defined as secant slope between (0,0) and the point when backbone curve have 0.75 of the maximum lateral strength. The yield displacement then defined from the intersection of initial stiffness with horizontal line of peak lateral load. Equation for calculating the yield displacement is:

$$K_i = \frac{0.75\,F_{max}}{0.75\,\delta_y} = \frac{F_{max}}{\delta_y} \qquad (1)$$

Thus, positive and negative direction of loadings is analyzed separately due to the difference of peak lateral load and initial slope of the curve. Normalization process for the backbone curve is summarized in the

Figure 8. Subsequently, comparison of significant yield points for each specimens are shown in Table 6.

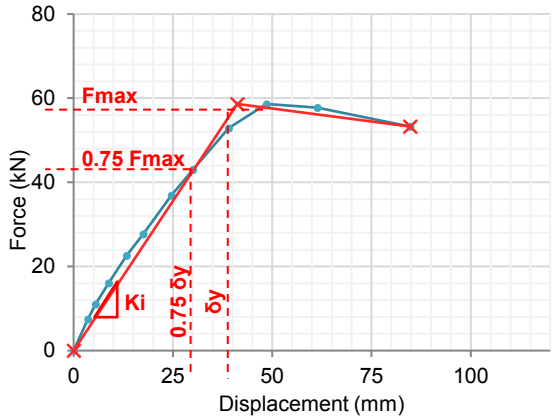

Figure 8. Normalization process of backbone curve

From the table, significant yield point of the specimen shifted to a higher value of lateral force and displacement by the change of yield strength. Furthermore, the addition of polypropylene fiber into concrete mixes of specimens can shift the significant yield point to a lower value of yield displacement, thus increasing the initial stiffness K_i of specimens.

Table 6. Significant yield point comparison

Specimens	Significant Yield			
	(+) dir.		(-) dir.	
	Displ. (mm)	Force (kN)	Displ. (mm)	Force (kN)
D16-400N	28.048	36.843	28.825	43.346
D16-500N	41.749	57.991	41.198	58.621
D16-500F	39.948	62.355	39.473	60.856
D19-500N	39.447	65.555	41.925	64.704
D19-500F	38.947	64.325	39.237	67.172

With the utilization of significant yield point explained above, comparison of energy dissipated by each specimen can be done. Energy dissipated by D16-400N and D16-500N specimens are compared in Figure 9. No noticeable difference was found in normalized dissipated energy between the specimens of conventional and high strength reinforcing bar. Difference in the yield displacement ratio of D16-400N and D16-500N specimens is due to difference in significant yield displacement, around 28 mm and 41 mm respectively.

As can be seen in Figure 5, all specimens are experiencing pinching at the end of the testing. This phenomenon indicating that all specimens, including the fibrous specimens, experiencing bond degradation of the beam longitudinal bars embedded in joint region. The amount of degradation for all specimens are shown in Table 11.

As expected, a higher capacity of dissipated energy was achieved in two fibrous concrete specimens, D16-500F and D19-500F. Improvement in energy dissipation capacity is due to the addition of polypropylene fiber that dissipating more energy by improving the bond of fiber and surrounding concrete. Energy dissipated by fibrous specimen of D16-500F is 24.5% higher than specimen with plain concrete D16-500N, whereas fibrous specimen of D19-500F is 27.5% higher than D19-500N specimen on the 3.5% drift level. Energy dissipated by each specimen with high strength steel is compared in Figure 10. Detailed comparison of energy dissipated by plain and fibrous specimens is shown in Table 7.

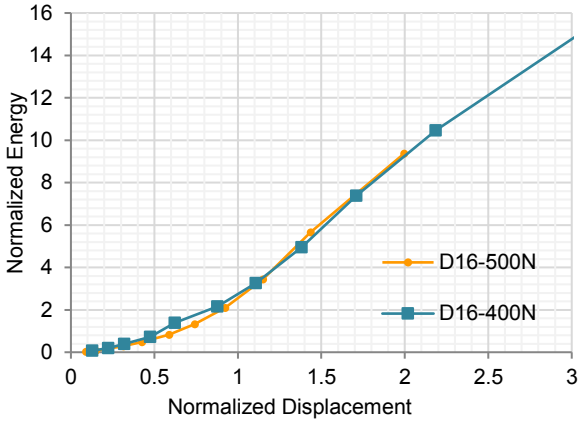

Figure 9. Cumulative dissipated energy comparison of conventional and high strength steel

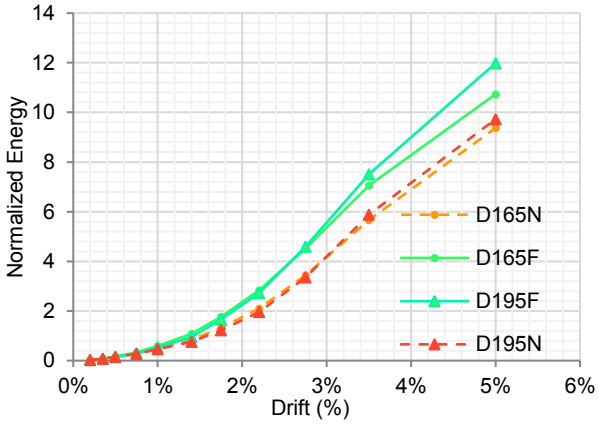

Figure 10. Cumulative dissipated energy comparison of plain and fibrous concrete

Table 7. Normalized dissipated energy comparison

Specimens	Drift 3.5%		Drift 5%	
	Norm. Energy	Ratio	Norm. Energy	Ratio
D16-500N	5.658	1.000	9.371	1.000
D16-500F	7.046	1.245	10.732	1.145
D19-500N	5.885	1.000	9.727	1.000
D19-500F	7.501	1.275	11.982	1.232

3.3 Peak-to-peak stiffness

From the backbone curve, difference in the rate of stiffness degradation by all specimens can be evaluated. This degradation can be due to bond loss between concrete and rebar, concrete cracking and spalling, etc. Peak-to-peak stiffness is defined as the slope of line that connecting two peak points (i.e.

* Corresponding author: maulanaderry@gmail.com

positive and negative loading direction) in the same cycle.

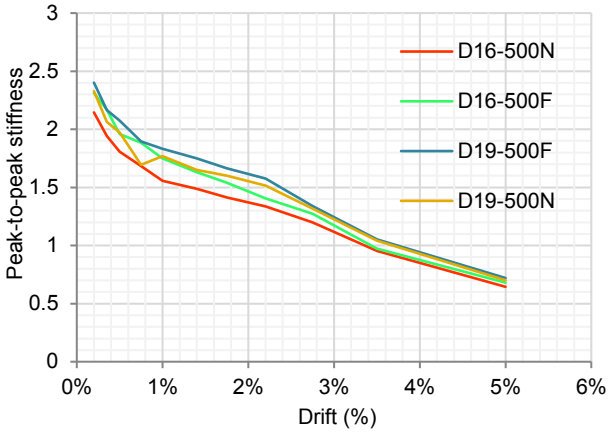

Figure 11. Peak-to-peak stiffness degradation

Peak-to-peak stiffness is improved in both fibrous concrete specimens. This improvement is observed to occur throughout the testing, although the magnitude of improvement varies along the test. For D16 specimens, the addition of polypropylene fiber enhances the initial stiffness by 7.8%, whereas an enhancement of 3.2% achieved by D19-500F specimen compared to that of specimens with plain concrete. Those initial stiffness is calculated from first cycle in the first drift level of the tests, i.e. at 0.2% drift level. At the end of loading, improvement of stiffness in fibrous concrete specimens is 5.6% and 2.7% over the stiffness of plain concrete specimens, for D16 and D19 specimens respectively. The comparison graph shown below suggested that the addition of concrete fiber is significantly enhancing the stiffness of specimens, notably in the elastic range loading. While for higher drift ratio the addition of fiber into concrete matrix increase the stiffness in a lower magnitude. Degradation of peak-to-peak stiffness of the specimens is illustrated in Figure 11.

3.4 Crack Pattern Analysis

The shape of cracks forming on the beams was documented throughout the testing. Documentation and measurement of those crack was done every at every peak or reversal in the cyclical loading. The pattern of cracks formed in plastic hinge region of the beams is shown in the Figure 12. Those pictures representing the beams condition in the last cycle loading, i.e. third cycle at 5% drift.

Specimens with fibrous concrete shows a more dispersed cracks formed in the beams relative to specimens with plain concrete. Moreover, no spalling was observed to take place in the plastic hinge region for fibrous concrete until the end of the test. The number and average spacing of the cracks on each specimen is quantified in Figure 13.

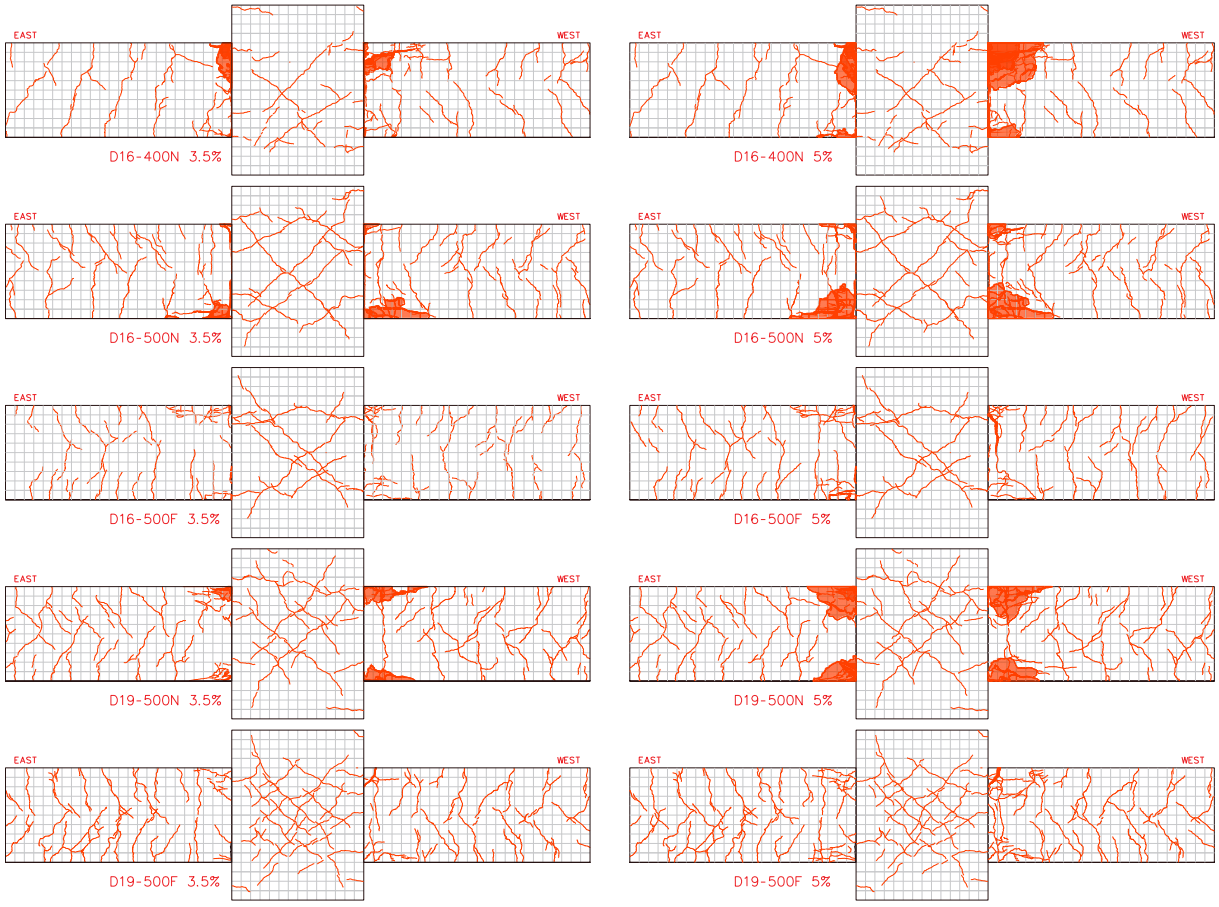

Figure 12. Cracks pattern comparison for D16-400N, D16-500N, D16-500F, D19-500N, and D19-500F specimens.

* Corresponding author: maulanaderry@gmail.com

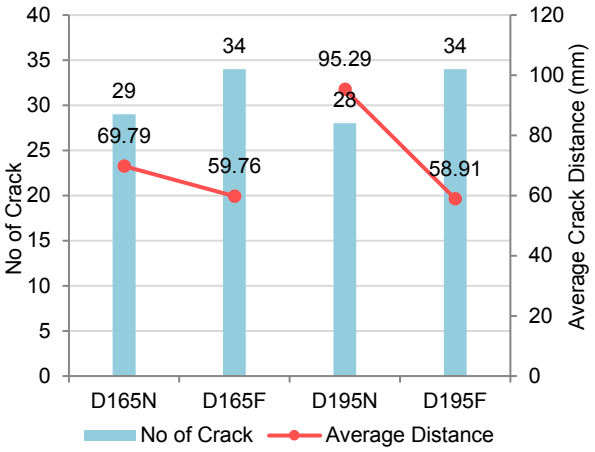

Figure 13. Number and distance of cracks comparison with the addition of fiber

Specimens with the addition of fiber were forming a higher number of cracks along the beam. The increase in number of cracks means the reduction of crack's spacing. The number of cracks formed in fibrous specimens is 17.2% and 21.4% higher for D16-500F and D19-500F specimens, compared to the number of cracks formed in specimens with plain concrete. The reduction in average spacing is 14.4% for D16-500F specimen, and 61.76% for D19-500F specimen. The enhancement of number of cracks formed or the reduction of cracks spacing, suggesting that the fibrous concrete has an improved bond capacity between concrete and reinforcing bars.

In addition to number and distance of the cracks, width of cracks also measured throughout the testing at several locations. Eight cracks were measured in each specimen at every reversal of the loading. The result of crack width, illustrated in Figure 14, shows that the smaller cracks were formed in fibrous specimens. Average width of the cracks formed in fibrous specimen is 18.62% smaller at the end of loading, or at 5% drift level. The comparison graph of crack width also suggested that the most significant reduction of crack width is at the elastic range loading.

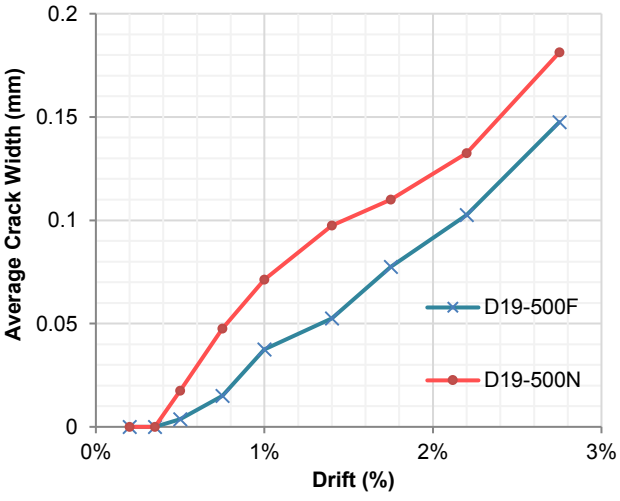

Figure 14. Crack width comparison of D19-500N and D19-500F specimens

3.5 Bond Analysis

Bond degradation is inevitable in a beam-column joint region during a monotonic or cyclical loading. The loss of bond between concrete and steel rebar could significantly decrease stiffness of elements in a small range of drift after a major earthquake. To measure the change of bond behavior after the addition of polypropylene fiber into concrete matrix, four strain gauges attached to longitudinal reinforcing bars inside the joint region is utilized.

Four strain gauge channels, numbered 20-24 according to Figure 2, took strains of rebar inside the joint region. Those recorded strains along the testing then converted into stress-strain history using Menegotto-Pinto cyclical steel model. From the calculated stresses, axial force of rebar in each location of strain gauge is acquired by multiplying the stresses with the area of rebar.

The bond of reinforcing bars and the surrounding concrete, τ, is calculated by dividing the difference of force of the two adjacent strain gauges, namely F_1 and F_2, with the area of contact between concrete and rebar, i.e.:

$$\tau = \frac{F_{s1} \cdot F_{s2}}{\pi \, d_s \, l_0}$$

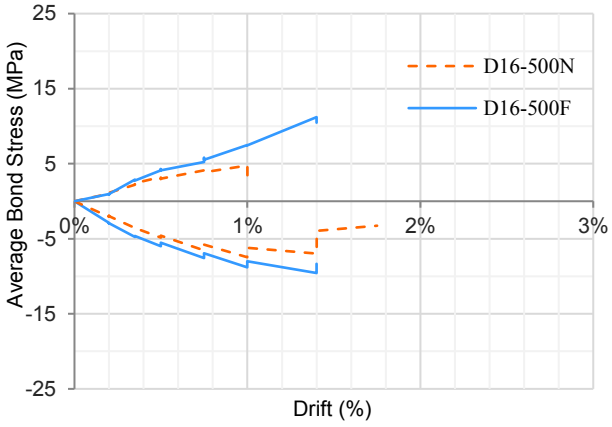

(a)

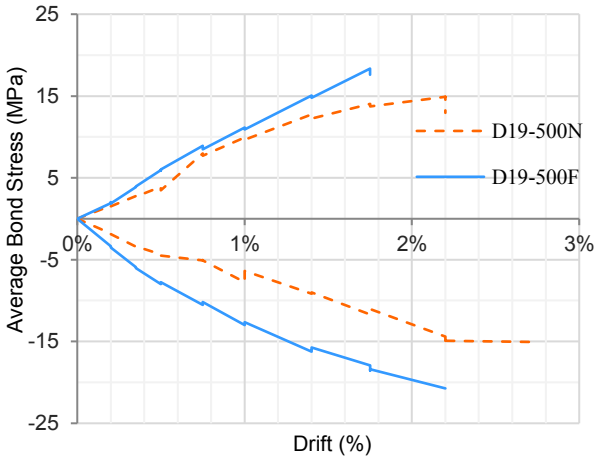

(b)

Figure 15. Average bond stress comparison for top reinforcing bars between (a) D16 specimens (b) D19 specimens

* Corresponding author: maulanaderry@gmail.com

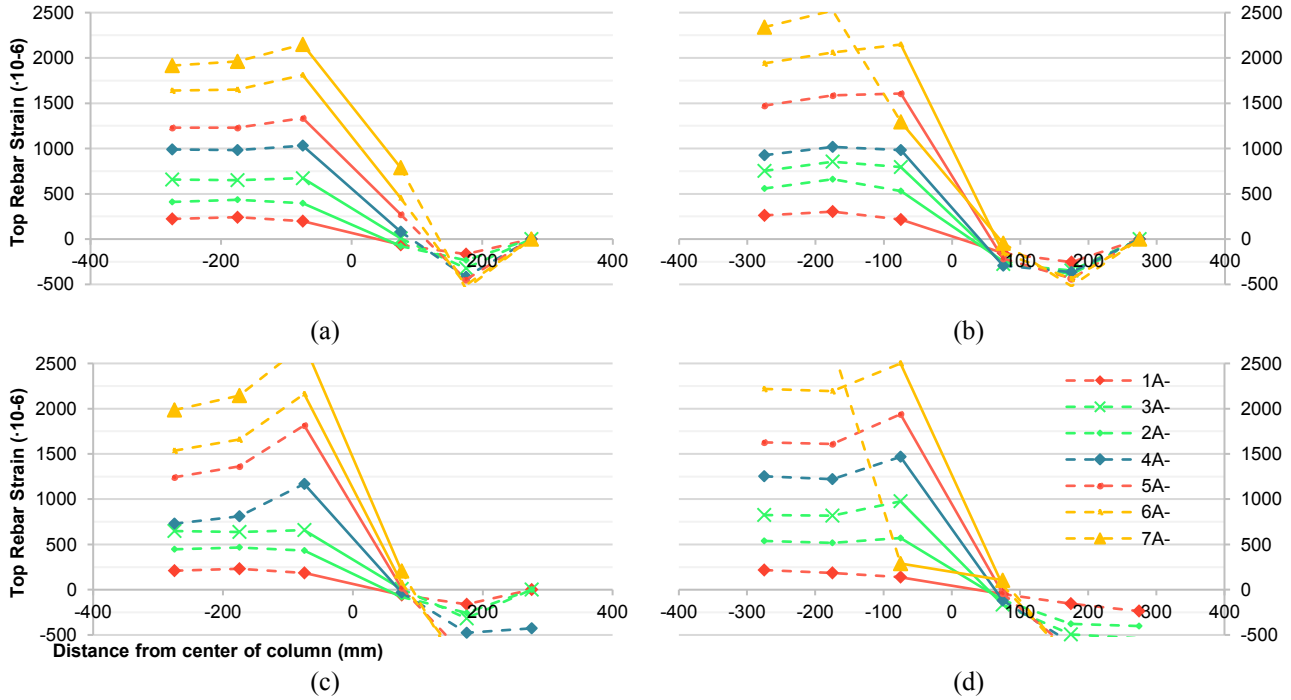

Figure 16. Strain profile for top reinforcing bars, (a) D16-500N (b) D16-500F (c) D19-500N (d) D19-500F

The area of contact is defined as the circumference of rebar's section, and multiplied by the distance of both strain gauges l_0, which is 150 mm in all specimens of this experimental program. It must be noted that the bond calculated above is an average value along the rebar between two strain gauges.

Result of bond calculation at the peak cycle load for top rebar is given in the Figure 15. While for bottom rebar, one of the two strain gauges installed in both D16-500F and D19-500F was malfunctioned from the beginning of the test, leading a high inaccuracy of calculated average bond in the bottom rebar. Also, due to the malfunctioning of strain gauges, measurement of average bond stress was stopped at the drift ratio around 1.4% - 2.2%, as the measurement of strains beyond those drift level is considered to be inaccurate due to the damage of strain gauges.

From the comparison graph above, it is evident that the specimens with fibrous concrete have a higher bond stress for the same loading level compared to the bond stress in the specimens with plain concrete. The increase measured in D16 specimens is 56.9% in 1% drift and 37.55% in 1.4% drift for positive and negative loading respectively. While for D19 specimens, average bond stress is increased about 30.88% in 1.75% drift and 48.92% in 2.2% drift, for positive and negative loading respectively.

3.6 Acceptance Criteria (ACI 374.1-05)

To ensure that the structure element tested is adequate for high seismic risk region, result obtained from laboratory testing then checked against the acceptance criteria explained in ACI 374.1-05 [6]. Three criteria that must be satisfied, according to the standard, is strength, energy, and stiffness.

3.6.1 Strength Criteria

To validate the strong column/weak beam behavior of the specimens, the maximum lateral load resistance of each specimen E_{max} shall less than λE_n. E_n is the nominal strength of the specimen obtained from calculation with strength reduction factor of 1, and λ is the specified column overstrength factor. Positive and negative loading directions are checked independently due to the possibility of difference in E_{max} between both loading directions. Maximum lateral loads checking are shown in Table 8.

All specimens pass this criterion as the maximum lateral loads E_{max} is less than the value of λE_n. Shown in the table below, all specimens have a high value of λ. Those high values of λ are intended to impel the beam flexural failure of the specimens, rather than any column-related failure.

Table 8. Maximum lateral loads criterion checking

Specimens	λ	λEn (kN)	Emax (kN)	
			(+) dir	(-) dir
D16-500N	2.106	94.103	58.621	57.991
D16-500F	2.106	94.103	60.856	62.355
D19-500N	3.015	94.103	64.704	65.555
D19-500F	3.015	94.103	67.172	64.325

In addition to maximum lateral load, strength degradation is another criterion that must be satisfied by the specimens. Strength degradation of specimens is checked at the third cycle of 3.5% drift level or higher, with minimum value of 0.75 E_{max}. The strength degradation checking for all specimens is shown in Table 9. All specimens pass the strength ratio criterion of ACI 374.1-05.

* Corresponding author: maulanaderry@gmail.com

Table 9. Strength ratio checking at third cycle at 3.5% drift ratio

Specimens	*Ultimate*		*3.5% C*	
	Drift (%)	*Force (kN)*	*Force (kN)*	*Strength ratio > 0.75*
D16-500N	3.50%	57.991	49.820	0.86
	2.75%	-58.621	-49.800	0.85
D16-500F	3.50%	62.355	50.591	0.81
	2.75%	-60.863	-45.674	0.75
D19-500N	2.75%	65.555	52.428	0.80
	3.50%	-64.704	-52.876	0.82
D19-500F	2.75%	64.325	50.496	0.79
	2.75%	-67.172	-54.852	0.82

3.6.2 Ideal Energy Ratio Criterion

To ensure the tested structure elements have adequate damping after an earthquake, relative energy dissipation ratio at the third cycle of 3.5% drift level or higher must exceed 0.125. If a structure element does not satisfy this criterion, structure will undergo an excessive oscillation for a while prior to an earthquake.

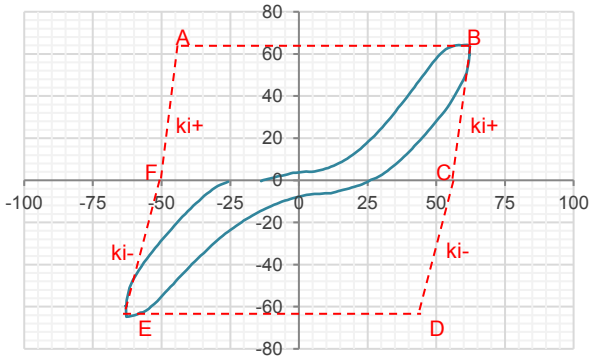

Figure 17. Ideal energy parallelograms ACI 374.1-05

Ideal energy is defined as the area of two parallelograms, namely ABCF and CDEF in Figure 17. Each parallelogram circumscribed by 2 horizontal lines and 2 parallel lines with slope of initial stiffness K_i. Definition of the parallelograms are shown in Figure 17, and ideal energy ratio of the specimens are shown in Table 10. All specimens must have an ideal energy ratio greater than 0.125 at every third cycle of 3.5% drift level or higher. From the table below, all specimens pass the criterion of ideal energy ratio, as the ratio of all specimens are greater than 0.125.

Table 10. Ideal energy ratio checking at third cycle of 3.5% drift ratio

Specimens	**3.5% C**	
	β	**Remarks**
D16-500N	0.1972	OK
D16-500F	0.1904	OK
D19-500N	0.2381	OK
D19-500F	0.2627	OK

* Corresponding author: maulanaderry@gmail.com

3.6.3 Secant Stiffness

After an earthquake, damaged structure is susceptible of undergo a large displacement due to a small lateral load. To prevent the small stiffness around small drift after a major earthquake, stiffness of specimens in near-zero drift must be greater than 0.05 of the initial stiffness. Two points at the drift of -0.35% to 0.35% creating secant stiffness that must satisfy the minimum secant stiffness criterion. Checking of each specimen regarding to this criterion can be seen in Table 11. From the table below, all specimens satisfy this criterion.

Table 11. Secant stiffness checking at third cycle of 3.5% drift ratio

Specimens	**Initial Stiffness**	**Drift 3.5% C**	
		Stiffness	**Ratio**
D16-500N	2079.894	113.415	0.055
	2058.808	105.798	0.051
D16-500F	2230.352	137.692	0.062
	2250.612	118.172	0.053
D19-500N	2294.065	116.714	0.051
	2281.971	136.202	0.060
D19-500F	2543.989	191.787	0.075
	2360.224	152.814	0.065

4 CONCLUSIONS

Five specimens, half-scaled models, were casted with the variation of yield strength of reinforcement bars used. Two of them were casted with fibrous concrete, using polypropylene fiber with 0.5% volumetric ratio. All specimens subjected to identical cyclic loading to make a comparative study. Interpretation of the data obtained from the testing is as follow:

- Specimens with the addition of polypropylene fiber have an increased maximum resisted lateral force, ranging from 4.5% to 8.4%. No spalling observed in the fibrous specimens.
- Both of fibrous specimens dissipated a higher energy than the specimens with plain concrete is. The energy dissipation enhancement is ranging from 24.5% to 27.5%.
- Stiffness of the specimens was increased with the addition of fiber into concrete mixes. Initial stiffness of fibrous specimens is 7.8% higher, and at the end of loading, peak-to-peak stiffness of fibrous specimens is 5.6% higher than specimens with plain concrete is. The most significant enhancement in stiffness is inside the elastic range.
- From the comparison of cracks formed on the beams, specimens with fibrous concrete have a larger number of cracks forming, and a reduced average spacing between cracks. Crack width is also reduced with the addition of fiber into concrete matrix.

- Specimens casted with fibrous concrete have a higher bond stress, at least up to 2.5% drift level as the strain measurement of reinforcing bars beyond this drift is not possible. The improvement of bond stress is ranging between 30.88% - 56.9%.
- All of the specimens tested satisfy the criteria specified in ACI 374.1-05, hence the structural elements tested in this research are validated to be used in the regions of high seismic risk.

REFERENCES

1. L. I. Osorio, P. Paultre, R. Eid and J. Proulx, "Seismic Behavior od Synthetic Fiber-Reinforced Circular Columns," *ACI Structural Journal,* pp. 189-200, 2014.
2. V. Ramakrishnan, G. Y. Wu and G. Hosalli, "Flexural Behavior and Toughness of Fiber Reinforced Concretes," Naval Facilities Engineering Command, 1989.
3. F. F. Wafa, "Properties and Applications of Fiber Reinforced Concrete," *Journals of King Abdulaziz University,* vol. 2, pp. 49-63, 1990.
4. S. Jie and C. Yin, "Stress Strain Behavior of Steel-Polypropylene Hybrid Fiber Reinforced Concrete Under True Triaxial Compression," in *5th International Conference on Civill Engineering and Transportation*, Guangzhou, 2015.
5. L. Huang, Y. Chi, L. Xu, P. Chen and A. Zhang, "Local Bond Performance of Rebar Embedded in Steel-Polypropylene Hybrid Fiber Reinforced Concrete Under Monotonic and Cyclic Loading," *Construction and Building Materials,* vol. 103, pp. 77-92, 2016.
6. K. Muthuswamy and G. Thirugnanam, "Structural Behavior of Hybrid Fibre Reinforced Concrete Exterior Beam-Column Joint Subjected to Cyclic Loading," *International Journal of Civil And Structural Engineering,* vol. 4, no. 3, pp. 262-273, 2014.
7. P. Perumal and B. Thanukumari, "Use of Fibre Cocktails to Increase the Seismic Performance of beam-Column Joints," *International Journal of Engineering Science and Technology,* vol. 2, no. 9, pp. 3997-4006, 2010.
8. N. Ganesan, P. Indira and R. Abraham, "Steel Fibre Reinforced High Performance Concrete Beam-Column Joints Subjected to Cyclic Loading," *ISET Journal of Earthquake Technology,* vol. 44, no. 4, pp. 445-456, 2007.
9. ASTM International, Standard Specification for Deformed and Plain Billet-Steel Bars for Concrete Reinforcement (ASTM A615M-03a), West Conshohocken: ASTM International, 2003.
10. ASTM International, Standard Specification for Low-Alloy Steel Deformed and Plain Bars for Concrete Reinforcement (ASTM A706M-04a), West Conshohocken: ASTM International, 2004.
11. ACI Committee 374, Acceptance Criteria for Moment Frames Based on Structural testing and Commentary (ACI 374.1-05), Farmington Hills: American Concrete Institute, 2005.

* Corresponding author: maulanaderry@gmail.com